JOURNAL OF AIRCRAFT
Vol. 45, No. 2, March–April 2008

Design Space Exploration of Supersonic Formation Flying Focusing on Drag Minimization

Yuichiro Goto,* Shinkyu Jeong,† Shigeru Obayashi,‡ and Yasuaki Kohama§
Tohoku University, Sendai 980-8577, Japan

DOI: 10.2514/1.28766

This study investigates the drag characteristics of a supersonic formation-flying concept that aims to reduce wave drag and sonic boom via shock-wave and expansion-fan interaction. Because of the complex interaction patterns seen in three-aircraft formations, optimization was applied as a rational means for design. To consider both the cruise efficiency and the safety of the aircraft, the objective functions are chosen to be the total L/D of the formation and the minimum separation distance among the aircraft. The design variables define the relative positions of the aircraft and, as for the coordinate definition, the skewed cylindrical coordinate system that has been proven to be very effective in extracting the physics of the flowfield was chosen. Optimization results show a good correlation with results from previous studies. However, optimization arrived at a formation that unexpectedly achieved high performances in regions of the design space in which the previous study suggested bad performance. These solutions took advantage of the design space of three-aircraft formations (i.e., the synergistic effects of the flowfield of the two leading aircraft) and exploited the difference between the design space of two-aircraft formations.

Nomenclature

C_D	=	drag coefficient
C_L	=	lift coefficient
C_M	=	pitching moment coefficient
C_p	=	pressure coefficient
c	=	chord length
$\boldsymbol{c}$	=	vector of Lagrange multipliers
d	=	distance between two aircraft
d'	=	weighted distance between two aircraft
F	=	coordinate conversion function from the skewed cylindrical coordinate definition to the Cartesian coordinate definition
f	=	objective function
g	=	constraint function
i_{cone}	=	position of the origin of the coordinate definition, expressed in aircraft number
M	=	freestream Mach number
n	=	number of samples
$\boldsymbol{R}$	=	matrix of correlation between the evaluated Z
$\boldsymbol{r}$	=	vector of correlation between the evaluated Z
r, θ, x_μ	=	coordinate parameters for the skewed cylindrical coordinate system
s	=	root mean squared error
T_t	=	wind-tunnel total temperature
u	=	unknown function of interest
$\boldsymbol{u}$	=	vector of evaluated function values
$\hat{u}$	=	kriging model of the unknown function
$u_{\max}$	=	maximum value among the evaluated samples
w	=	z direction component of the local velocity
$\boldsymbol{x}$	=	dependent variables of the unknown function
x, y, z	=	coordinate parameters for the Cartesian coordinate system
Z	=	random deviation from the constant global model
α	=	angle of attack
δ	=	weighted distance in the dependent parameter space
μ	=	Mach angle
ν	=	constant global model to model for the unknown function
Σ	=	weighting parameter for the weighted distance
Φ	=	cumulative distribution function
ϕ	=	probability density function

Subscripts

i, j	=	aircraft number
0	=	aircraft 0, the leading aircraft
1	=	aircraft 1, the first following aircraft
2	=	aircraft 2, the second following aircraft

Superscript

0	=	coordinate definition converted back to $i_{\text{cone}} = 0$

I. Introduction

IN THE past 50 years, many attempts have been made to realize commercially practical civil supersonic transports. The two major problems that have prevented supersonic commercial transportation are wave drag and sonic boom. Wave drag, which is the dominating component of drag at supersonic speeds, leads to a deterioration in cruise efficiency. And sonic booms have a problem of public acceptance, which leads to strict route limitations.

Many attempts have been made to minimize the wave drag and the sonic boom via aircraft shape optimization. However, results have shown a strong tradeoff between wave drag and sonic boom, making it impossible to minimize wave drag and sonic boom simultaneously.

As a different approach to overcoming these problems, the use of formation flying in supersonic speeds for the simultaneous reduction of wave drag and sonic boom was proposed [1]. The reduction of sonic boom is achieved via favorable wave interference. When aircraft fly through the air at supersonic speeds, they leave momentum in the air behind them. This is the cause of wave drag. The wave drag of the following aircraft is reduced by collecting this momentum as a pressure gradient. The reduction of sonic boom of the fleet is achieved by virtual elongation. It is a well-known fact that the pressure signature of the sonic boom is dependent on the overall

Received 8 November 2006; accepted for publication 19 August 2007. Copyright © 2007 by the authors.. Published by the American Institute of Aeronautics and Astronautics, Inc., with permission. Copies of this paper may be made for personal or internal use, on condition that the copier pay the $10.00 per-copy fee to the Copyright Clearance Center, Inc., 222 Rosewood Drive, Danvers, MA 01923; include the code 0021-8669/08 $10.00 in correspondence with the CCC.

*Currently Research and Development Engineer, Bosch Corporation. Member AIAA.
†Associate Professor, Institute of Fluid Science, 2-1-1 Katahira Aoba-ku. Member AIAA.
‡Professor, Institute of Fluid Science, 2-1-1 Katahira Aoba-ku. Associate Fellow AIAA.
§Professor, Institute of Fluid Science, 2-1-1 Katahira Aoba-ku.

length and the area distribution of the aircraft. This area distribution is defined by a sweep of a plane inclined downward at the Mach angle. If the aircraft are placed in a way such that the area distribution of the aircraft are clustered together, this will result in an elongated pressure wave, consequently reducing the boom intensity.

Research on favorable wave interference dates back to the 1930s, when Busemann proposed the "Busemann biplane" [2], which takes advantage of the shock-wave interaction between the upper and lower wings of a biplane to cancel out the wave drag of the configuration at a zero-lift condition in linear theory. In the 1950s, the numerous research on favorable wave interference were carried out. Here, interference of the shock wave from various components of the aircraft was used to reduce the wave drag of the entire configuration. For example, Friedman and Cohen [3] carried out linear analyses on bodies of revolution, imitating a fuselage and stores. As a result, they have shown that wave drag per total cross-sectional area can be reduced when placed in an optimal relative position. Positions of the stores that were favorable for wave-drag reduction were positions at which the stores were placed inside a shock wave, which is a positive pressure jump. The shock wave that impinges on the stores generate thrust, canceling a part of their drag. Recently, Kusunose et al. [4] presented an extensive analysis on the Busemann biplane, intending actual application to supersonic transport aircraft. However, in these concepts, the aircraft tend to become very unconventional in configuration and tend to lose the benefits of design. On the other hand, the supersonic formation-flying concept incorporates more flexibility in the configuration, overcoming these difficulties.

As a first step to understanding the effectiveness of the supersonic formation-flying concept, analysis has been carried out on two-aircraft formations to investigate the sensitivity of wave drag with respect to the relative position of the aircraft [1]. Results showed that the Mach cone extending from the leading aircraft plays an important role in the drag reduction, and results showed similar trends along the same Mach cone. In two-aircraft formations, the flow pattern was simple and intuitive, and the formations in the analysis were generated from intuition on the flowfield.

The objective of the current study is to extend this study to three-aircraft formations and gain insight on the drag reduction of three-aircraft formations. The relation between the relative position of the three aircraft and the drag reduction of each of the aircraft will be investigated. Especially, discovery of three-aircraft formations that achieve high performance, which are in a formation particular to three-aircraft formations and cannot be predicted from the results of two-aircraft formations, is also expected.

Because the flow patterns are expected to be more complicated and less intuitive in three-aircraft formations, it is impractical to generate the formations from intuition, as done in the previous study. Therefore, in this study, design is carried out in a more objective manner. For objective design, optimization using kriging is carried out. Kriging [5] was chosen taking into account the fact that expensive Euler computations are used for the flow analysis. This method makes it possible to optimize the formation to a certain level in a limited amount of computation.

II. Problem Definition

The objective of the supersonic formation-flying concept is to reduce the total wave drag of the formation. However, in realizing actual formation flying, the safety and the control effort needed for the position keeping is also an important factor. Therefore, in this study, the objectives are chosen to be the maximization of the total L/D of the formation and the maximization of the minimum of the separations between the aircraft. The first objective is considered for improving the cruise efficiency, and the second objective is considered to maximize the safety and the tolerance of the position keeping.

The objective of this study is to investigate the change in the preceding objective functions with respect to the relative positions of the aircraft. Therefore, the design variables are the variables defining the position of the two following aircraft, whereas the leading aircraft stays at the origin.

In the coordinate system used in this analysis, x is in the freestream direction, y is out toward the right wing tip, and z is upward. The origin of the coordinate system is located at the half-chord position along the centerline of the leading aircraft. The coordinates are normalized by the root chord of the aircraft.

The previous study [1] showed that shock interaction is the most important physics in drag reduction, and the skewed cylindrical coordinate expression was proposed to effectively extract the physics. This coordinate definition will be used as the design variables that define the relative position of the aircraft. The conversion from the cylindrical coordinate expression to the Cartesian expression for aircraft i is given by

$$\begin{aligned} x_i &= x_{i_{\text{Cone}}} + x_{\mu i} + r_i/\tan\mu \\ y_i &= y_{i_{\text{Cone}}} + r_i \sin\theta \\ z_i &= z_{i_{\text{Cone}}} - r_i \cos\theta \end{aligned} \tag{1}$$

where $x_{i_{\text{Cone}}}$, $y_{i_{\text{Cone}}}$, and $z_{i_{\text{Cone}}}$ are the position of aircraft i_{cone}, which is the origin of coordinate definition for aircraft i; r_i is a parameter to express how far away the following aircraft is located along the Mach cone from the leading aircraft; θ_i is the azimuthal position in the y–z plane; and $x_{\mu i}$ expresses the streamwise position of the following aircraft with respect to the Mach cone extending downstream from the center of the leading aircraft. Although there are small discrepancies due to nonlinearity, x_μ can be regarded as a parameter that indicates how the following wing interacts with the shock and expansion waves. More specifically, if $x_\mu \approx -0.5$, then the upstream half of the following wing will be in undisturbed freestream and the leading-edge shock of the leading aircraft will be impinging near the midchord point of the following aircraft, and if $x_\mu \approx 0.0$, the leading-edge shock of the leading aircraft will be impinging near the leading edge of the following aircraft, and so on.

The leading aircraft, aircraft 0, is defined as the origin of the coordinate system. Next, the coordinates of the first following aircraft, aircraft 1, are defined by the three parameters given earlier, with the origin of coordinate definition placed at aircraft 0. Finally, the coordinates of the second following aircraft, aircraft 2, are given by the three preceding parameters and an integer variable i_{cone_i}, defining which aircraft the origin of the coordinate definition is placed upon. In general, the integer variable i_{cone_i} takes an integer value from the range $[0, i-1]$ for aircraft i. This coordinate definition makes it possible to effectively cover the coordinate space in which we expect shock interaction and, at the same time, to exclude regions in which we expect no shock interaction.

Figures 1a and 1b are diagrams showing the relation between the Cartesian coordinate system and the coordinate definition used in the optimization for $i_{\text{cone}} = 0$ and $i_{\text{cone}} = 1$, respectively. In these figures, the Cartesian coordinate system is drawn in black dashed

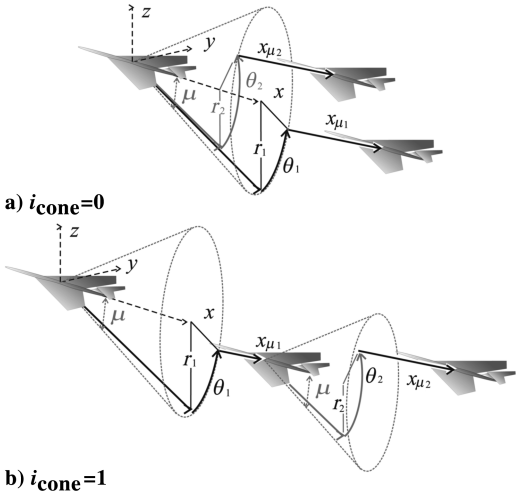

Fig. 1 Diagram of the skewed cylindrical coordinate definition.

Table 1 Design variables and their bounds

Variable	Type	Bounds
r_1	real	[0, 3.0]
θ_1	real	[−4.0, 4.0]
$x_{\mu 1}$	real	[−2.0, 2.0]
r_2	real	[0, 3.0]
θ_2	real	[−4.0, 4.0]
$x_{\mu 2}$	real	[−2.0, 2.0]
i_{cone_2}	integer	[0,1]

lines, the Mach cone is drawn in gray dotted lines, and the definition of the coordinate definition is drawn in black solid lines for aircraft 1 and gray solid lines for aircraft 2. The number of design variables was seven. The design variables and their upper and lower bounds are given in Table 1.

The constraints imposed on the positions of the aircraft were only geometrical constraints; that is, the aircraft must stay inside the outer boundary of the computational mesh, and the aircraft must be a certain distance away from each other. These constraints were imposed to ensure successful generation of the computational mesh. The mesh outer boundary was a conical shape with the apex at (−3.5, 0.0, 0.0), and the base is a circle, with its center located at (5.0, 0.0, 0.0), with a radius of 8.5. As for the distance between the aircraft, an ellipsoid that is able to enclose the aircraft with a small margin is selected. Weights are given to each of the components of the coordinate system so that the ellipsoid in the original coordinate system is mapped as a sphere in the weighted coordinate system. This mapped coordinate system is used to define the distance between the aircraft. Readers should note that this weighted coordinate system is only used in defining the distance between the aircraft in the constraint, but not in the objective function.

Finally, the problem can be given in the following form.

$$\begin{aligned} &\text{maximize } f_1 = \sum_i L_i / \sum_i D_i \\ &\text{maximize } f_2 = \min_{i,j,i\neq j} d_{i,j} \end{aligned} \tag{2}$$

$$\begin{aligned} \text{subject to} \quad & g_1 = \min_i x^0_{\mu i} > -2.5 \\ & g_2 = \max_i x_i < 4.0 \\ & g_3 = \min_{i,j,i\neq j} d'_{i,j} > 2.0 \end{aligned} \tag{3}$$

where

$$(r^0_i, \theta^0_i, x^0_{\mu i}) = \boldsymbol{F}_0^{-1}[\boldsymbol{F}_{i_{\text{cone}}}(r_i, \theta_i, x_{\mu i})] \tag{4}$$

$$d_{i,j} = (x_i - x_j)^2 + (y_i - y_j)^2 + (z_i - z_j)^2 \tag{5}$$

$$d'_{i,j} = [(x_i - x_j)/1.0]^2 + [(y_i - y_j)/1.2]^2 + [(z_i - z_j)/0.1]^2 \tag{6}$$

Here, $\boldsymbol{F}_{i_{\text{cone}}}$ is the coordinate conversion function defined in Eq. (1), and r^0_i, θ^0_i, and $x^0_{\mu i}$ are the cylindrical coordinate parameters converted to $i_{\text{cone}_2} = 0$. Because the only value of i_{cone} belongs to aircraft 2, for simplicity, i_{cone_i} will be called i_{cone} from here on.

III. Method

A. Optimization

Optimization is carried out using a combination of Latin hypercube sampling, kriging, and multi-objective genetic algorithm, with expected improvement as the objectives. The steps of the optimization are given next.

1) Generate initial solutions.
2) Evaluate objective and constraint function values.
3) Generate a response surface.
4) Evaluate the estimated objective values and the uncertainties to choose new solutions to add to the response surface.
5) If satisfied with the accuracy, exit; else, go to step 2.

The initial solutions are generated using Latin hypercube sampling. This sampling technique ensures that the range of all of the design variables are covered using all of the generated solutions. Here, it was ensured that the solutions satisfy the constraints. The objective and constraint functions are evaluated using an Euler flow solver and simple geometry, respectively. Details on the flow solver will be mentioned in Sec. III.B.

Next, the response surface is generated from the solutions using kriging. Kriging is a statistics-based response surface method that is able to estimate both the function values and their uncertainties. In this method, the unknown function of interest is expressed as

$$u(\boldsymbol{x}) = \nu + Z(\boldsymbol{x})$$

where ν is a constant global model for the unknown function, and $Z(\boldsymbol{x})$ is the random deviation from that model. To model this function, a linear predictor

$$\hat{u} = \boldsymbol{c}^T(\boldsymbol{x})\boldsymbol{u}$$

is identified by minimizing the mean squared error subject to an unbiasedness constraint, using Lagrange multipliers and an optimality condition [6]. Here, $\boldsymbol{u}$ is the vector of the evaluated function values. Then the kriging model used in this study is obtained in the following form.

$$\hat{u} = \hat{\nu} + \boldsymbol{r}^T\boldsymbol{R}^{-1}(\boldsymbol{u} - \mathbf{1}\hat{\nu})$$

where

$$\hat{\nu} = \frac{\mathbf{1}^T\boldsymbol{R}^{-1}\boldsymbol{u}}{\mathbf{1}^T\boldsymbol{R}^{-1}\mathbf{1}}$$

The mean squared error is given by

$$s^2(\boldsymbol{x}) = \hat{\sigma}^2\left[1 - \boldsymbol{r}^T\boldsymbol{R}^{-1}\boldsymbol{r} + \frac{(1 - \mathbf{1}^T\boldsymbol{R}^{-1}\mathbf{1})^2}{\mathbf{1}^T\boldsymbol{R}^{-1}\mathbf{1}}\right]$$

where

$$\hat{\sigma}^2 = \frac{(\boldsymbol{u} - \mathbf{1}\hat{\nu})^T\boldsymbol{R}^{-1}(\boldsymbol{u} - \mathbf{1}\hat{\nu})}{n}$$

$\boldsymbol{R}$ is the matrix of correlation between the evaluated Zs, and $\boldsymbol{r}$ is the correlation vector between the Z to be estimated and the evaluated Z. Because the correlation of Z is strongly dependent on the distance between the two solutions, a weighted distance and a Gaussian random function will be used as the correlation.

$$\delta(\boldsymbol{x_i}, \boldsymbol{x_j}) = (\boldsymbol{x}_i - \boldsymbol{x}_j)^T\boldsymbol{\Theta}(\boldsymbol{x}_i - \boldsymbol{x}_j)$$

where $\boldsymbol{\Theta}$ is a matrix with the weights as the diagonal elements. Using this weighted distance, the correlation will be defined as

$$\text{corr}\,[Z(\boldsymbol{x}_i), Z(\boldsymbol{x}_k)] = \exp[-\delta(\boldsymbol{x}_i, \boldsymbol{x}_j)]$$

$\boldsymbol{r}$ and $\boldsymbol{R}$ can finally be written as

$$\boldsymbol{r}_j(\boldsymbol{x}) = \exp[-\delta(\boldsymbol{x}, \boldsymbol{x}_j)] \qquad \boldsymbol{R}_{i,j} = \exp[-\delta(\boldsymbol{x_i}, \boldsymbol{x}_j)]$$

The log-likelihood function of the sampled solutions can be written as

$$-\frac{n}{2}\ell_n(2\pi) - \frac{n}{2}\ell_n(\hat{\sigma}^2) - \frac{1}{2}\ell_n(|\boldsymbol{R}|) - \frac{1}{2\hat{\sigma}^2}(\boldsymbol{u} - \mathbf{1}\hat{\nu})^T\boldsymbol{R}^{-1}(\boldsymbol{u} - \mathbf{1}\hat{\nu})$$

Therefore, the problem will be an unconstrained optimization problem of minimizing

$$-\frac{n}{2}\ell_n(\hat{\sigma}^2) - \frac{1}{2}\ell_n(|\boldsymbol{R}|)$$

with respect to the weighting parameter matrix $\boldsymbol{\Theta}$. In the current problem definition, design variable i_{cone} is an integer variable. Therefore, the kriging surface is generated separately for each value i_{cone} takes for each objective function.

To evaluate the estimated objectives and the uncertainties simultaneously, a figure of merit called *expected improvement* is used [7]. Expected improvement is a parameter that considers both the uncertainty and the objective function itself. In case of a maximization problem, expected improvement is defined as

$$\text{EI}(\boldsymbol{x}) = E[\max(Z - u_{\max}, 0)]$$

where $y_{\max}$ is the maximum objective value of the sampled solutions. Solving for the expected value, the expected improvement results in

$$\text{EI}(\boldsymbol{x}) = (\hat{u} - u_{\max})\Phi\left(\frac{\hat{u} - u_{\max}}{s}\right) + s\phi\left(\frac{\hat{u} - u_{\max}}{s}\right)$$

where ϕ and Φ are the probability density function and the cumulative distribution function of the Gaussian distribution. The process of maximizing the expected improvement is carried out via genetic algorithm for use in multi-objective problems [5]. Fonseca–Fleming's Pareto ranking method is used in this genetic algorithm, because this method is more is proven to be more effective in generating solutions sparsely over the frontier of nondominated solutions.

Finally, to evaluate the convergence of the kriging model, cross validation is carried out by excluding and estimating one sampled solution and comparing their values.

As mentioned before, i_{cone} is an integer parameter. Integer problems are basically a combinatorial problem and thus make the optimization complex. Especially, in the current optimization method, a response surface is used to model the objective function with respect to the design variables. Therefore, if i_{cone} is also left in the response surface mode, the model would be modeling an integer variable using a smooth function. Therefore, this variable will make the response surface misleading for the optimizer to carry out the search. However, for the current problem, i_{cone} only takes two values: 0 or 1. Therefore, in this section, a separate optimization will be carried out for $i_{\text{cone}} = 0$ and $i_{\text{cone}} = 1$, and the results from each of the optimizations will be compared.

B. Flow Computation

Because the objective of this study is to investigate the effectiveness of supersonic formation flying, the subject of the analysis is kept simple. For this reason, the model used for this study is a simple elliptical planform wing with a biconvex airfoil. The flowfield around a biconvex airfoil is an upstream shock wave followed by an expansion fan, finally ending with the trailing-edge shock. This pattern is much simpler than that of a wing–body configuration, eliminating the need to account for interaction with multiple shock waves and expansion fans.

Although simplification of the configuration is convenient, the drag characteristics of the simplified model must be similar to that of a practical supersonic transport. The aspect ratio and the thickness are determined so that the lift-dependent wave drag, volume-dependent wave drag, and vortex drag are close to that for a wing–body diagram, estimated by a simple drag model [1]. This resulted in an elliptic wing with the following dimensions: aspect ratio of 1.5, normalized span of $1.5\pi/4$, thickness ratio of 0.04502, and wing area of 0.9253. A three-view diagram of this configuration is given in Fig. 2.

The freestream Mach number used in this analysis is $M = 1.5$. This Mach number was chosen considering recent trends in the cruise Mach number of recent supersonic transport concepts. The angles of attack of the wings are maintained at $\alpha = 3.25$ deg.

The computational mesh used in this analysis is an unstructured full three-dimensional mesh with 1.05 million grid points and 42,000 grid points on each wing. The cross section of this mesh at $y = 0$ is given in Fig. 3. A full three-dimensional mesh is used to allow for asymmetric formations.

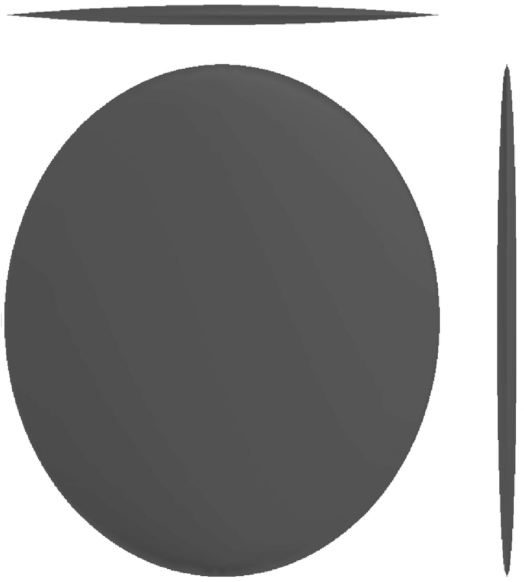

Fig. 2 Three-view diagram of the simplified model.

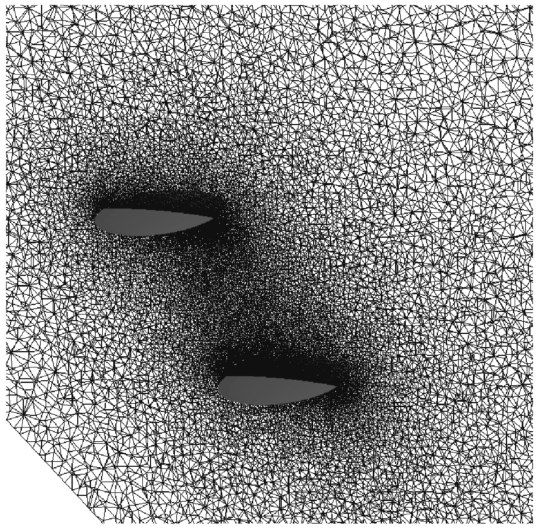

Fig. 3 Symmetry plane of computational mesh.

Euler simulations are carried out using TAS-flow, an unstructured Euler/Navier–Stokes solver, and the computational mesh was generated using EdgeEditor and TU TetraGrid, which are computational fluid dynamics tools developed at Tohoku University.

TAS-flow is an unstructured Euler/Navier-Stokes solver using a finite volume cell-vertex scheme, Harten–Lax–van Leer–Einfeldt–Wada (HLLEW) Riemann solver for flux computations [8], and lower–upper symmetric Gauss–Seidel (LU-SGS) implicit scheme for time integration [9]. EdgeEditor is an unstructured surface mesh generation software. It takes CAD data as input [10] and generates a surface mesh using an advancing-front triangulation method [11]. TU TetraGrid is an unstructured volume mesh generation software using the Delaunay triangulation algorithm [12].

IV. Results and Discussion

A. Generated Solutions and Nondominated Solutions

All of the solutions obtained from the optimization are shown in Fig. 4. The solutions are plotted to the two objective functions and shaded by their Pareto ranking. Figure 4a is for $i_{\text{cone}} = 0$, and Fig. 4b is for $i_{\text{cone}} = 1$. The first objective function is the total L/D of all aircraft and will be called f_1 from here on. The second objective is the

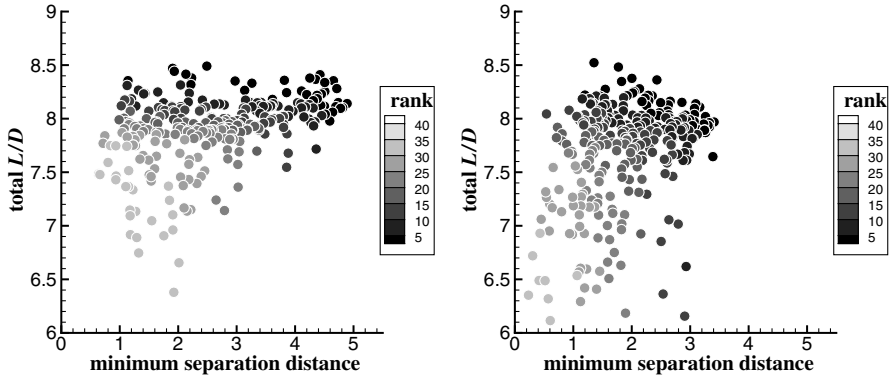

a) $i_{\text{cone}} = 0$ b) $i_{\text{cone}} = 1$

Fig. 4 All solutions plotted to the two objective functions and shaded by their Pareto ranking.

minimum separation distance between the aircraft and will be denoted as f_2. The solutions are plotted to the two objective functions, f_1 and f_2. The value of f_1 of the nondominated solutions take very similar values for both values of i_{cone}. The value of f_1 when flying in a formation without shock-wave and expansion-fan interaction is 7.89. This value will be used as the baseline value in the discussion. Comparing this baseline value with the solutions plotted in Fig. 4, the figure indicates that the gains in L/D of the well-performing formations are much smaller than the losses in performance of the inferior formations. This is due to the fact that the interaction with the component of shock waves and expansion fans related to the generation of lift only contains a downward momentum, which only acts to reduce the lift, thus reducing the L/D. Therefore, the aircraft must be positioned in such a way that it interacts with the volume-dependent component of the shock waves and expansion fans. Although the gains and losses in L/D were similar to both values of i_{cone}, the upper limit of f_2 is constrained at a much lower value for $i_{\text{cone}} = 1$. This is due to the fact that because aircraft 2 is located on the Mach cone of aircraft 1, aircraft 2 must be located downstream of aircraft 1, making it difficult to obtain streamwise separation.

To clarify the mechanism of the improvements in the performance, the strong nondominated solutions will be investigated.

In Figs. 5 and 6, solution 144 for $i_{\text{cone}} = 0$ and 262 for $i_{\text{cone}} = 1$ are plotted, respectively. These are the formations that achieved the highest values for f_2 for each value of i_{cone}. Flow is into the paper for front-view figures.

First, solution 144 for $i_{\text{cone}} = 0$ is investigated. The numbers of the objective functions, the design variables, and the performance of each of the aircraft are given next.

$$f_1 = 8.14 \quad r_1 = 3.00 \quad r_2 = 2.77 \quad C_{L_0} = 0.145$$
$$C_{D_0} = 0.0184 \quad L/D_0 = 7.89 \quad f_2 = 4.89 \quad \theta_1 = 0.21\pi$$
$$\theta_2 = -0.71\pi \quad C_{L_1} = 0.156 \quad C_{D_1} = 0.0188 \quad L/D_1 = 8.32$$
$$x_{\mu_1} = 0.34 \quad x_{\mu_2} = 0.87 \quad C_{L_2} = 0.148 \quad C_{D_2} = 0.0180$$
$$L/D_2 = 8.21$$

The isosurface in the figure indicates the surface on which $C_p = -0.015$ (i.e., indicating the position of the expansion fan in the flowfield). It can be seen in Fig. 6 that the following aircraft are obtaining the gain in performance from the expansion fan from aircraft 0. However, the way the aircraft achieves its high performance is different. Aircraft 1, which is flying lower than aircraft 0, is using the expansion fan to obtain enough lift to compensate for the increase in drag. On the other hand, because the expansion fan acts to reduce the lift when flying above, aircraft 2 takes a higher value for x_μ. This means that aircraft 2 is not flying so far inside the expansion fan so that the impinging expansion fan reduces the drag but does not greatly reduce the lift. Having the shock wave after the expansion fan impinging on the lower surface compensates for the loss in lift due to the expansion fan.

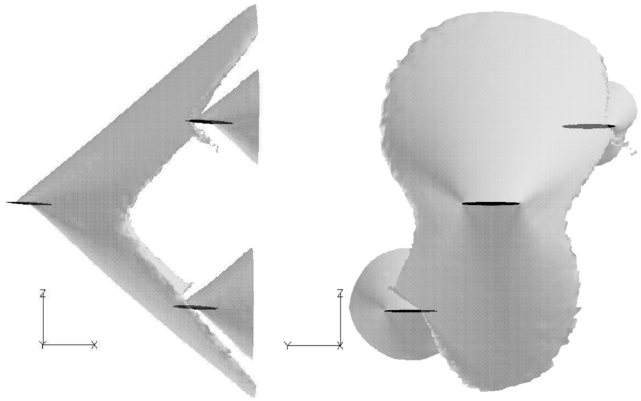

a) Side view b) Front view

Fig. 5 Isosurface shows the surface for $C_p = -0.015$; solution 144.

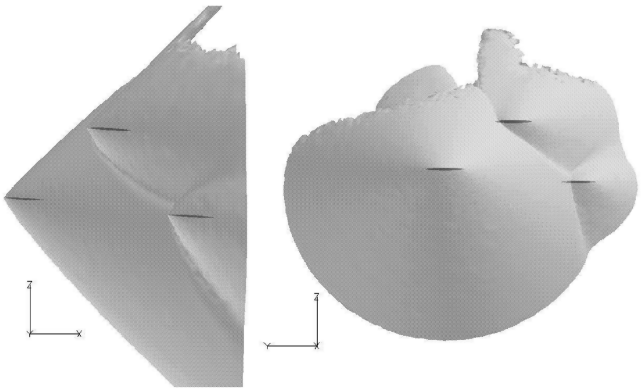

a) Side view b) Front view

Fig. 6 Isosurface shows the surface for $C_p = 0.005$; solution 262.

As for solution 262 for $i_{\text{cone}} = 1$, the numbers for the formation are

$$f_1 = 7.97 \quad r_1 = 2.71 \quad r_2 = 2.99 \quad C_{L_0} = 0.145$$
$$C_{D_0} = 0.0184 \quad L/D_0 = 7.90 \quad f_2 = 3.41 \quad \theta_1 = -0.70\pi$$
$$\theta_2 = -0.27\pi \quad C_{L_1} = 0.149 \quad C_{D_1} = 0.0186 \quad L/D_1 = 8.02$$
$$x_{\mu_1} = -0.97 \quad x_{\mu_2} = -1.51 \quad C_{L_2} = 0.141 \quad C_{D_2} = 0.0176$$
$$L/D_2 = 7.99$$

In this case, as stated before, aircraft 2 must basically fly downstream of aircraft 1 (the way to gain separation is to have aircraft 2 fly as far downstream as possible), and after that, aircraft 1 must fly as far as

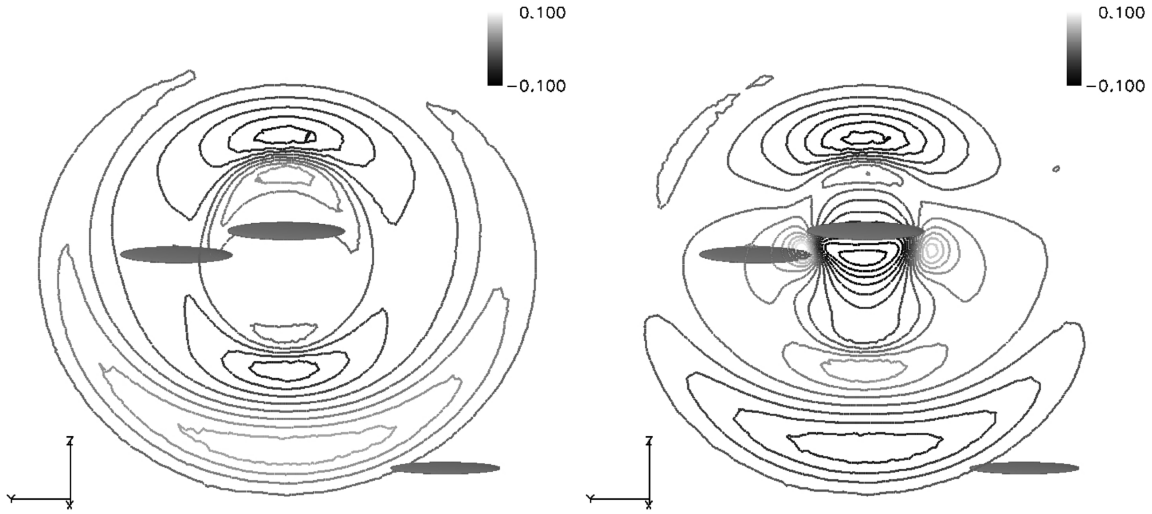

a) C_p distribution **b) Upwash distribution**

Fig. 7 Flowfield in the plane at the leading edge of the aircraft that achieved the highest value of L/D; solution 110 for $i_{\text{cone}} = 0$.

possible from the two aircraft. Figure 6 shows the isosurface of $C_p = 0.005$. Examining this figure, the gain in L/D of the following aircraft are obtained from the interaction with the leading-edge shock wave of aircraft 0. As for aircraft 1, the shock wave impinges on the aircraft on the lower surface. This increases the lift and also increases the drag, but because the increase in lift is more effective than the increase in drag, the L/D increases. Aircraft 2, on the other hand, has the shock wave impinging on the aft half of the upper surface, acting to reduce the drag and also to reduce the lift. In this case, the effect on the lift is less effective than the effect on the drag and therefore increases the L/D. These four figures indicate that the gain in L/D is obtained by interaction with the shock waves and the expansion fans of aircraft 0. These results are consistent with the insight obtained in the previous study [1].

Next, the formations that achieved the best value for f_1 is investigated for $i_{\text{cone}} = 0$ and $i_{\text{cone}} = 1$. Solution 110 for $i_{\text{cone}} = 0$ and solution 106 for $i_{\text{cone}} = 1$ are visualized in Figs. 7 and 8. In both cases, one of the following aircraft achieved an extremely high L/D, whereas the other following aircraft did not achieve such a high L/D. To investigate the cause of this extremely high L/D, the flowfield near the aircraft that achieved the highest L/D among the fleet is visualized. Here, the C_p distribution and upwash distribution is visualized at a plane perpendicular to the freestream, located at the leading edge of the aircraft that achieved the highest L/D among the aircraft in the fleet. Upwash is defined as the z component of the local flow velocity. Freestream direction is tilted slightly away from the reader for all figures. This was done to avoid the overlapping of aircraft as much as possible.

Numbers for solution 110 for $i_{\text{cone}} = 0$ are given next.

$f_1 = 8.49 \quad r_1 = 2.73 \quad r_2 = 1.15 \quad C_{L_0} = 0.145$

$C_{D_0} = 0.0184 \quad L/D_0 = 7.89 \quad f_2 = 2.49 \quad \theta_1 = -0.22\pi$

$\theta_2 = 0.51\pi \quad C_{L_1} = 0.153 \quad C_{D_1} = 0.0183 \quad L/D_1 = 8.36$

$x_{\mu_1} = 0.59 \quad x_{\mu_2} = 0.92 \quad C_{L_2} = 0.188 \quad C_{D_2} = 0.0206$

$L/D_2 = 9.14$

In this formation, aircraft 1 is the lower aircraft on the starboard side, and aircraft 2 is the aircraft on the port side, as shown in Fig. 7. The position of aircraft 1 is very similar to the position of aircraft 1 of solution 144, as seen in Fig. 5, and also the gain in performance is very similar. Therefore, the mechanism for the enhancement in performance of the case stated earlier can be used to explain the current case. In this solution, the isosurface of C_p was generated and the drag-reduction mechanism of aircraft 1 was confirmed to be similar to the drag-reduction mechanism seen in solution 144. The C_p distribution, Fig. 7a, indicates that the aircraft is flying in a position in which the expansion fan, shown in the darker shade, is very weak at this azimuthal position and passes by just upstream of the leading edge, missing the aircraft. Therefore, little advantage is gained from the interaction with the expansion fan. However, Fig. 7b indicates that the aircraft is flying inside the upwash of the leading aircraft, aircraft 0. The L/D of this aircraft, achieving its benefit from the trailing vortex, is comparable with the best solutions in the previous study [1], which obtained their benefit from shock-wave and expansion-fan interaction.

Numbers of solution 106 for $i_{\text{cone}} = 1$ are given next.

$f_1 = 8.52 \quad r_1 = 0.73 \quad r_2 = 0.74 \quad C_{L_0} = 0.145$

$C_{D_0} = 0.0184 \quad L/D_0 = 7.89 \quad f_2 = 1.35 \quad \theta_1 = -0.08\pi$

$\theta_2 = -0.46\pi \quad C_{L_1} = 0.162 \quad C_{D_1} = 0.0162 \quad L/D_1 = 9.81$

$x_{\mu_1} = 0.53 \quad x_{\mu_2} = -1.99 \quad C_{L_2} = 0.121 \quad C_{D_2} = 0.0153$

$L/D_2 = 7.92$

In this formation, aircraft 0 is the aircraft on top, aircraft 1 is the aircraft directly below, and aircraft 2 is the aircraft to the starboard side of aircraft 1, as shown in Fig. 7. Figure 8 shows the C_p distribution and upwash distribution in a plane at the leading edge of aircraft 1. Also, in this case, aircraft 1 achieved an extremely high L/D. The C_p distribution, Fig. 8a, shows a region of low pressure just above the leading edge of the wing, which indicates an expansion fan. Aircraft 1 uses this expansion fan from the aircraft flying above to reduce drag. Also, Fig. 8b suggests that aircraft 1 also uses the upwash from the aircraft flying to the starboard side, aircraft 2. By using both the expansion fan and the upwash, the aircraft achieved an L/D of 9.81, which corresponds to a 24% improvement from the baseline case.

In this case, aircraft 1 is taking a position in which aircraft 1 can interact with the expansion fan of aircraft 0 and at the same time be inside the trailing vortex of aircraft 2. This configuration is only possible for $i_{\text{cone}} = 1$, because $i_{\text{cone}} = 0$ basically does not permit one aircraft to line up behind another aircraft. Therefore, this is the explanation to the trend that $i_{\text{cone}} = 1$ is superior in effectively extracting momentum from the leading aircraft in a three-aircraft formation.

B. Drag-Reduction Mechanisms Particular to Three-Aircraft Formations

Next, the difference in the design space between two-aircraft formations and three-aircraft formations is investigated to search for

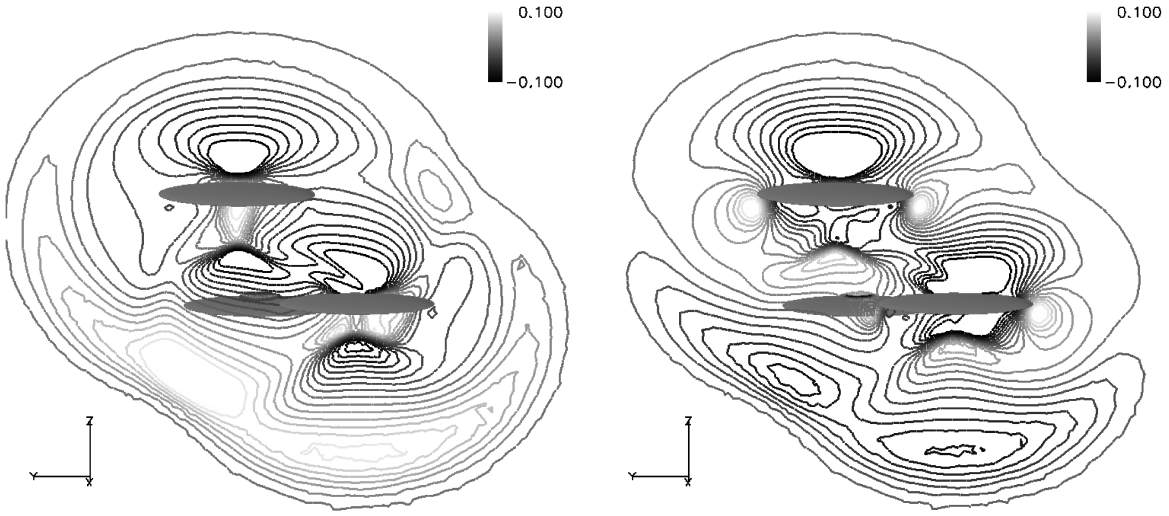

a) C_p distribution **b) Upwash distribution**

Fig. 8 Flowfield in the plane at the leading edge of the aircraft that achieved the highest value of L/D; solution 106 for $i_{\text{cone}} = 1$.

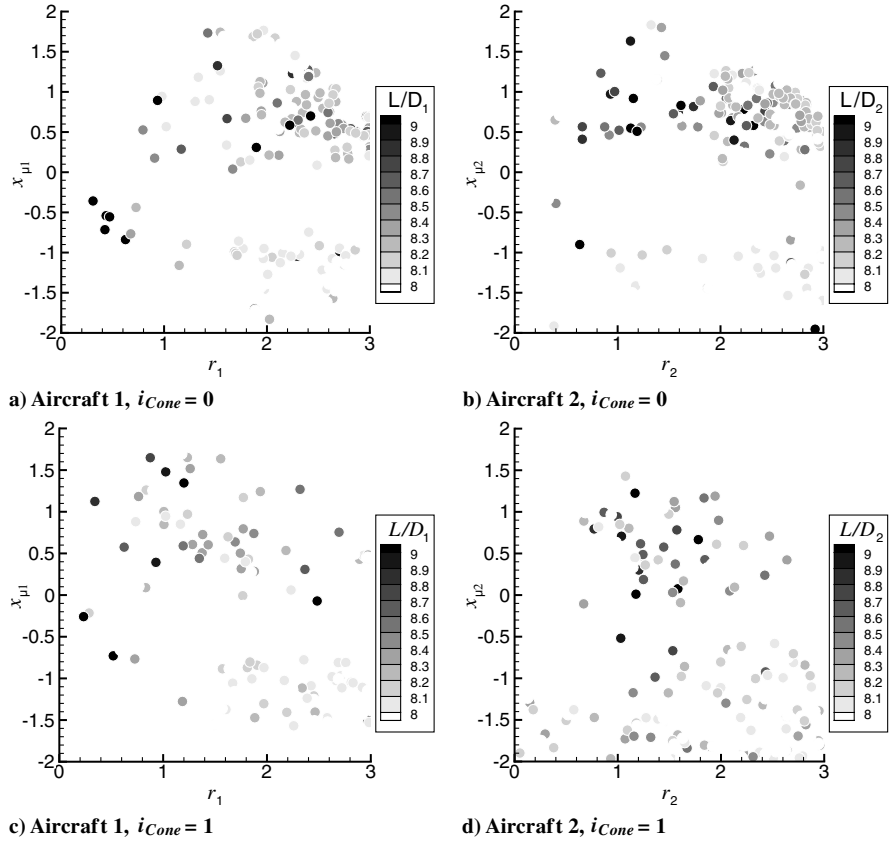

a) Aircraft 1, $i_{Cone} = 0$ **b) Aircraft 2, $i_{Cone} = 0$**

c) Aircraft 1, $i_{Cone} = 1$ **d) Aircraft 2, $i_{Cone} = 1$**

Fig. 9 Solutions plotted to the design variables for each aircraft shaded by the L/D of each of the aircraft.

drag-reduction mechanisms particular to three-aircraft formations. This is done by analyzing each of the following aircraft in the formation using knowledge from the previous study and picking up solutions that achieve a high performance that cannot be explained. For this, the solutions are plotted to the design variables for each aircraft, and they are shaded by the value of L/D of the aircraft. The plots are shown in Fig. 9. From the results of the optimization, there was very little correlation between the objective functions and the azimuthal parameter θ; therefore, the solutions are plotted to r and x_μ only. Here, the range of the legend is adjusted so that the solutions with an L/D lower than 8.0 are white, which practically erases the solutions on the map. Therefore, the visible solutions on the plots are the solutions that obtained an L/D that is better than the baseline value. The previous study [1] indicated that interaction with expansion fans results in an improvement of L/D and the interaction with shock waves results in deterioration. Figures 9a and 9b show this tendency very clearly. When $-0.5 \leq x_\mu \leq 0.0$, which indicates an interaction with the leading-edge shock wave, there are very few solutions that obtain good performance. On the other hand, when $0.0 \leq x_\mu \leq 0.5$, which indicates interaction with the expansion fan, the solutions achieved good performance. The same trend can be seen in Figs. 9c and 9d. However, in Fig. 9d, the trend is much weaker than in the other plots. This is due to the fact that when $i_{\text{cone}} = 1$, aircraft 2 flies on the Mach cone of aircraft 1. This means that

aircraft 2 has more freedom to interact with not only the pressure field of aircraft 1, but also with the pressure field of aircraft 0. This results in a much more complex interaction pattern, making it impossible to explain the interaction with only r and x_μ.

Next, individual solutions are investigated in detail. First, aircraft 1 of solution 198 for $i_{\text{cone2}} = 0$ achieves a high L/D value of 9.22. The objective value, the design variables, and the aerodynamic performance will be given next.

$f_1 = 6.45$ $r_1 = 0.47$ $r_2 = 1.28$ $C_{L_0} = 0.032$
$C_{D_0} = 0.0106$ $L/D_0 = 3.03$ $f_2 = 0.47$ $\theta_1 = -0.84\pi$
$\theta_2 = 0.98\pi$ $C_{L_1} = 0.174$ $C_{D_1} = 0.0188$ $L/D_1 = 9.22$
$x_{\mu_1} = -0.56$ $x_{\mu_2} = -0.59$ $C_{L_2} = 0.103$ $C_{D_2} = 0.0184$
$L/D_2 = 5.58$

The flowfield is shown in Fig. 10. The aircraft in the middle is aircraft 1, which is the aircraft that achieved a high L/D. In this case, aircraft 1 is positioned just upstream and very close to aircraft 0. This allows aircraft 1 to take advantage of the shock extending upward from the leading edge of aircraft 0 and to have the trailing edge miss the effect of the expansion fan that would otherwise be pulling aircraft 1 downward, degrading the performance. This trend can also be seen in the chordwise C_p distribution plot shown in Fig. 11. In this figure, the C_p distribution of aircraft 0 is compared with that of an aircraft flying in freestream. Here, the difference between the baseline case and aircraft 1 is the shock wave and the shock wave reflected off aircraft 0. These shock waves impinge on the lower surface, as seen also in Fig. 10. A very slight effect of the expansion fan is only seen very near the trailing edge, which indicates a small effect of loss in performance. Although this aircraft has a very good cruise performance, this performance is that being traded off with the performance of aircraft 0, because it has the shock wave impinging on the upper surface, greatly reducing the lift. Also, this positioning would have safety issues with the aircraft flying in a distance closer than the chord length of the aircraft. Investigating other formations in the regions $r < 1.0$ and $-1 < x_\mu < 0$, all formations that achieved a good performance were flying in a relative position that is very similar to the current formation. However, these solutions rarely came close to the nondominated solution, because the high performance of the aircraft of interest is trading off the performance of the other closely interacting aircraft.

Next, solution 010 for $i_{\text{cone2}} = 0$ is observed. Numbers for this solution are given next.

$f_1 = 8.18$ $r_1 = 2.71$ $r_2 = 1.17$ $C_{L_0} = 0.112$
$C_{D_0} = 0.0142$ $L/D_0 = 7.85$ $f_2 = 1.20$ $\theta_1 = -1.12\pi$
$\theta_2 = -1.16\pi$ $C_{L_1} = 0.124$ $C_{D_1} = 0.0139$ $L/D_1 = 8.92$
$x_{\mu_1} = -1.02$ $x_{\mu_2} = -1.59$ $C_{L_2} = 0.145$ $C_{D_2} = 0.0184$
$L/D_2 = 7.89$

The relative position of the aircraft can be identified in Fig. 12. In this formation, the aircraft are positioned such that the shock wave of aircraft 0 extends along the expansion fan of aircraft 2, as can be seen in Fig. 12. This creates a favorable pressure field (i.e., a pressure gradient that results in the generation of thrust). By having aircraft 1 fly inside this pressure field, thrust is generated on aircraft 1, canceling a part of its drag. The effect of this pressure field can be seen in the chordwise C_p distribution of aircraft 1, as shown in Fig. 13. The expansion fan impinging on aircraft 1 acts to reduce the pressure on the upstream half, but also reduces the lift. However, with the shock wave of aircraft 0 impinging on the aft half, the loss in lift is compensated and also contributes to a further reduction in drag.

A solution that had a very unique interaction pattern was solution 161 for $i_{\text{cone}} = 1$. The numbers for this formation are given next.

$f_1 = 8.48$ $r_1 = 2.17$ $r_2 = 1.18$ $C_{L_0} = 0.145$
$C_{D_0} = 0.0184$ $L/D_0 = 7.89$ $f_2 = 1.77$ $\theta_1 = -0.54\pi$
$\theta_2 = -0.49\pi$ $C_{L_1} = 0.151$ $C_{D_1} = 0.0188$
$L/D_1 = 8.04$ $x_{\mu_1} = -1.02$ $x_{\mu_2} = 0.01$ $C_{L_2} = 0.210$
$C_{D_2} = 0.0225$ $L/D_2 = 9.33$

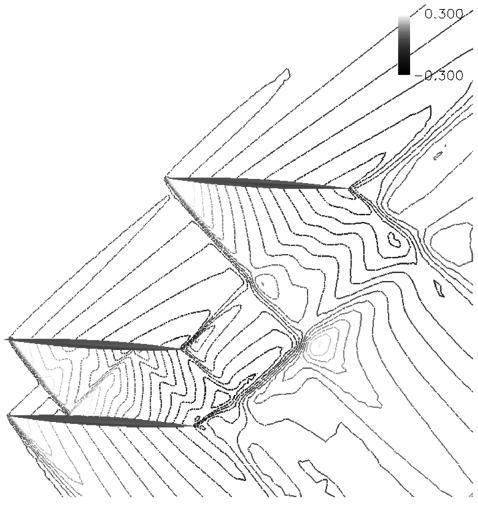

Fig. 10 C_p contour in the symmetry plane of aircraft 1; solution 198 for $i_{\text{cone2}} = 0$.

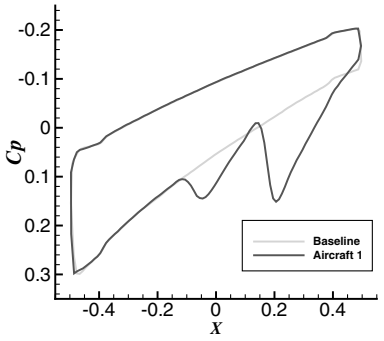

Fig. 11 C_p distribution of aircraft 1 at the wing root; solution 198 for $i_{\text{cone2}} = 0$.

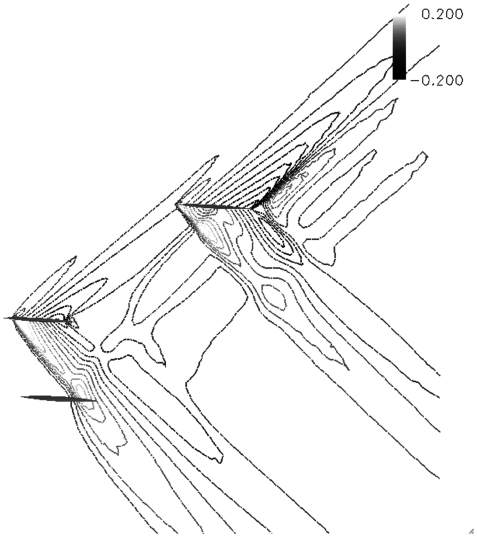

Fig. 12 C_p contour at the symmetry plane of aircraft 1; solution 010 for $i_{\text{cone2}} = 0$.

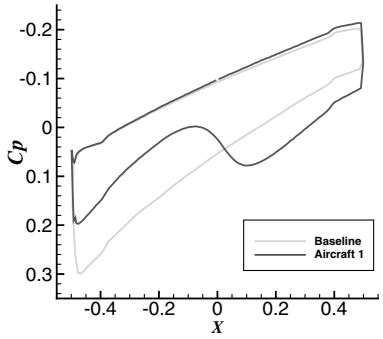

Fig. 13 C_p distribution of aircraft 1 at the wing root; solution 010 for $i_{\text{cone2}} = 0$.

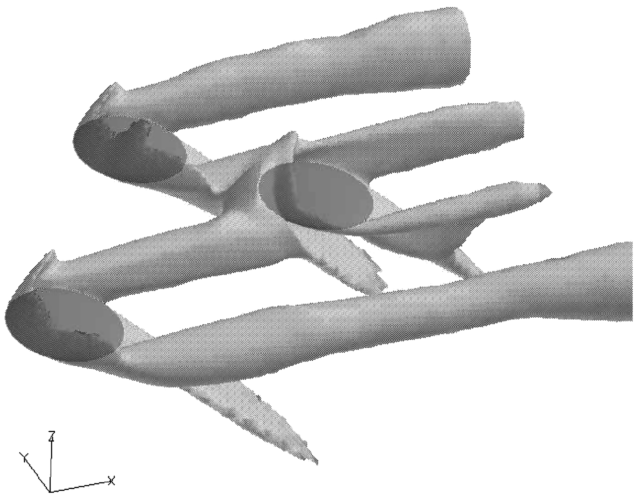

Fig. 14 Isosurface of $w = 0.03$; solution 161 for $i_{\text{cone2}} = 1$.

Aircraft 2 of this aircraft achieves an L/D of 9.33, although the value of x_μ is very close to 0.0. From the knowledge from the previous study, this would indicate the impinging of the shock wave near the leading edge, which would result in increase in drag. The flowfield is visualized in Fig. 14. Aircraft 2 is the aircraft that is positioned most downstream in this figure. Figure 14, which shows the isosurface of upwash velocity, indicates that the induced upwash field from the two leading aircraft merge and flows into aircraft 2. The lift generated by aircraft 2 is greatly enhanced due to this in-flowing strong upwash field. Aircraft 2 is also placed in a position such that it interacts with the shock wave generated by aircraft 0 (Fig. 15), although the drag-reduction effect is very small.

Looking at the solutions, it was possible to categorize most of the drag-reduction mechanisms of the unexpectedly performing aircraft into these three cases or a combination of these three.

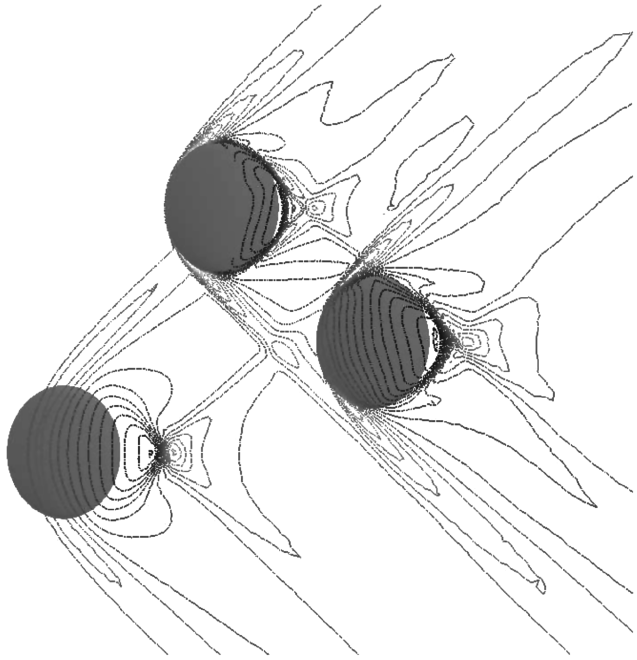

Fig. 15 C_p contour in the x–y plane at the z position of aircraft 2; solution 161 for $i_{\text{cone2}} = 1$.

C. Effect of the Interaction with Trailing Vortices.

The results from the optimization suggests that the enhancement in performance due to the induced upwash of the leading aircraft is comparable in magnitude with that due to the pressure field. Therefore, consideration for the reduction of vortex drag due to the induced upwash field is necessary in evaluating the drag reduction by supersonic formation flying. This characteristic will be investigated in this section.

The effect of spanwise position of the following aircraft on its aerodynamic performance is shown in Fig. 16. This analysis was carried out at $x = 3.5$ and $z = 0.0$. To separate the effect of the tip vortex and the shock wave, the downstream position was chosen so that the following aircraft will be well outside the vortex before interacting with the leading-edge shocks.

Looking at the figure, there is a very slight influence of shock-wave and expansion-fan interaction near $3.0 \leq y \leq 4.0$, but it is negligible compared with the overall trend. As expected, the value of C_L is very small due to the induced downwash at $y = 0.0$ (i.e., between the trailing vortices). The value of C_L increases as the following aircraft starts to interact with the induced upwash and takes a maximum value near $y = 1.0$, because the position of the wing tip of the leading aircraft is near $y = 0.59$. In this case, achieving the highest values of L/D, the aircraft is positioned well outside of the vortex center, which is assumed to be positioned downstream of the wing tip. Qualitatively, the same tendency can be seen in the variation of drag, but because the variation in drag is much smaller in

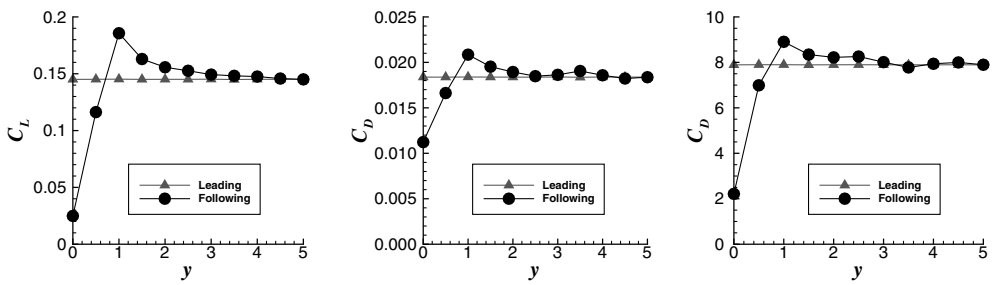

a) C_L **b) C_D** **c) *LbyD***

Fig. 16 The effect on aerodynamic performance, due to spanwise position of the following aircraft; $x = 3.9$ and $z = 0.0$.

fraction, the L/D varies in the same manner as the C_L. Quantitatively, the best value of L/D achieves about a 13% improvement. Therefore, the variation in aerodynamic performance due to the induced field is comparable with the variation in performance due to shock-wave and expansion-fan interaction.

V. Conclusions

In this study, the drag characteristics of a three-aircraft supersonic formation-flying concept was investigated. In the course of the investigation, optimization was carried out as a method of rational design. The objectives were chosen to be the total L/D of the fleet and the minimum separation distance between the aircraft, to consider both the cruise efficiency and the safety of the aircraft. The design variables are the parameters that define the relative positions of the aircraft in the formation. As for the definition of the position of the aircraft, the skewed cylindrical coordinate system was incorporated. This is a coordinate definition that was proven to conform well to the physics of the flow.

Comparing the results obtained from the two values of i_{cone}, $i_{\text{cone}} = 0$ was superior in achieving a high value for the minimum separation distance, and $i_{\text{cone}} = 1$ was superior in achieving a high total L/D, which resulted from a more effective use of both the expansion fan and the induced upwash. This indicates a need to consider the trailing vortices in the coordinate definition.

Looking at the nondominated solutions that were obtained by the optimization, the solutions that achieved the highest values of minimum separation took advantage of interaction with the expansion fan to increase its total L/D. However, the solutions that achieved the highest values for total L/D took advantage of the upwash induced by one of the tip vortices of the aircraft flying directly upstream. Also, the aircraft that achieved the highest value of total L/D used both the expansion fan and the induced upwash and achieved an increase in L/D of 24%, compared with an aircraft that is flying in undisturbed freestream.

The solutions from the optimization indicated that the relationship between the relative position and the aerodynamic performance is mostly similar to the relation obtained for two-aircraft formations. When $-0.5 \leq x_\mu \leq 0.0$, which indicates an interaction with the leading-edge shock wave, very few formations achieved an L/D that is better than an aircraft flying without interaction. Also, most of the solutions that achieved a good performance took values of x_μ higher than 0.0, which indicates an interaction with the expansion fan of the leading aircraft.

However, there were a few formations that unexpectedly achieved a good performance at values of x_μ that was thought not to be beneficial. In most of these formations, the last aircraft used the region in which a superposition of the flowfield from the two leading aircraft generates a synergistically advantageous flowfield. These formations exploited the difference between the design space of two-aircraft formations and that of three-aircraft formations.

The results from the optimization also suggested the importance of interaction with tip vortices. Many solutions that achieved a good performance took advantage of the induced upwash around the tip vortices. Finally, the effectiveness of the induced upwash on the performance of the following aircraft was investigated. Results suggested that the benefits from the upwash are comparable in magnitude with benefits from shock-wave and expansion-fan interaction.

This study, in collaboration with the previous study, succeeded in clarifying the mechanism of the drag reduction in supersonic formation flying. The knowledge obtained in the current study will be useful in the design of formations containing more aircraft or formations of aircraft with more complex configuration.

Acknowledgments

This work was supported by a 21st Century Center of Excellence (COE) program grant of the International COE of Flow Dynamics from Ministry of Education, Culture, Sports, Science and Technology. Authors would also like to thank K. Nakahashi and the Spacecraft Systems Laboratory, Department of Aerospace Engineering, Tohoku University for providing the computational fluid dynamics analysis tools.

References

[1] Goto, Y., Obayashi, S., and Kohama, Y., "Wave Drag Characteristics of a Low-Drag Supersonic Formation Flying Concept," *AIAA Journal*, Vol. 44, 2, 2007, pp. 675–679. doi:10.2514/1.23236

[2] Liepmann, H. W., and Roshko, A., *Elements of Gasdynamics*, Wiley, New York, 1957, pp. 116–118.

[3] Friedman, M. D., and Cohen, D., "Arrangement of Fusiform Bodies to Reduce the Wave Drag at Supersonic Speeds," NACA Rept. 1236, 1955.

[4] Kusunose, K., Matsushima, K., Goto, Y., Yamashita, H., Yonezawa, M., Maruyama, D., and Nakano, T., "A Fundamental Study for the Development of Boomless Supersonic Transport Aircraft," AIAA Paper 2006-0654, 2006.

[5] Jeong, S., Yamamoto, K., and Obayashi, S., "Kriging-Based Probablistic Method for Constrained Multi-Objective Optimization Problem," AIAA Paper 2004-6437, 2004.

[6] Sacks, J., Welch, W. J., Mitchell, T. J., and Wynn, H. P., "Design and Analysis of Computer Experiments," *Statistical Science*, Vol. 4, 4, 1989, pp. 409–435.

[7] Jones, D. R., Schonlau, M., and Welch, W. J., "Efficient Global Optimization of Expensive Black-Box Functions," *Journal of Global Optimization*, Vol. 13, No. 4, 1998, pp. 455–492. doi:10.1023/A:1008306431147

[8] Obayashi, S., and Guruswamy, G. P., "Convergence Acceleration of an Aeroelastic Navier-Stokes Solver," *AIAA Journal*, Vol. 33, 6, 1994, pp. 1134–1141.

[9] Sharov, D., and Nakahashi, K., "Reordering of Hybrid Unstructured Grids for Lower-Upper Symmetric Gauss–Seidel Computations," *AIAA Journal*, Vol. 36, 3, 1998, pp. 484–486.

[10] Ito, Y., and Nakahashi, K., "Surface Triangulation for Polygonal Models Based on CAD Data," *International Journal for Numerical Methods in Fluids*, Vol. 39, 1, 2002, pp. 75–96. doi:10.1002/fld.281

[11] Ito, Y., and Nakahashi, K., "Direct Surface Triangulation Using Stereolithography Data," *AIAA Journal*, Vol. 40, 3, 2002, pp. 490–496.

[12] Sharov, D., and Nakahashi, K., "A Boundary Recovery Algorithm for Delaunay Tetrahedral Meshing," *Numerical Grid Generation in Computational Field Simulations*, Mississippi State Univ., Mississippi State, MS, 1996, pp. 229–238.